



Marginal-restraint mandrel-free spinning process for thin-walled ellipsoidal heads

Yong-Cheng Lin^{1,2,3} · Jia-Yang Chen^{1,2} · Dao-Guang He^{1,2} · Xin-He Li^{1,3} · Jian Yang³

Received: 16 August 2019/Revised: 2 January 2020/Accepted: 4 March 2020/Published online: 31 March 2020
© Shanghai University and Springer-Verlag GmbH Germany, part of Springer Nature 2020

Abstract Metal sheet spinning is an advanced near-net forming technology for the manufacture of thin-walled ellipsoidal heads. The exact control of dimensional accuracy, however, is a considerable problem for spinning thin-walled parts with large diameter-to-thickness ratios. In this work, a marginal-restraint mandrel-free spinning process with two passes is proposed for the fabrication of thin-walled ellipsoidal heads without wrinkling. A finite element model is established and verified to study the influences of spinning parameters on the dimensional precision of thin-walled ellipsoidal heads. It is found that the spinning parameters considerably influence the deviations of wall thickness and contour characteristics. A small forming angle or small roller fillet radius during the first pass spinning, as well as the small angle between passes or high feed ratio during the second pass spinning, can improve the wall thickness precision. Meanwhile, as the forming angle or feed ratio is increased during the first pass spinning, the contour precision initially increases and then decreases. During the second pass spinning, the contour precision can be improved at a small angle between passes, whereas it deteriorates at a larger roller installation angle. The

optimized spinning parameters are obtained and verified by experiments.

Keywords Alloy · Thin-walled ellipsoidal heads · Spinning · Finite element model · Dimensional precision

1 Introduction

In view of its high material utilization and flexibility, metal sheet spinning is regarded as an advanced near-net forming technology [1, 2]. For instance, metal sheet spinning is utilized to manufacture axisymmetric thin-walled parts, such as thin-walled ellipsoidal heads [3, 4]. These ellipsoidal alloy heads are widely used in aviation, aerospace, and chemical and nuclear industries, such as heads of rocket fuel tanks and pressure vessels [2, 5, 6]. Normally, the spinning parameters considerably influence the forming quality of thin-walled parts [5, 7]. If these parameters are not suitably employed, however, some forming defects, including wrinkling or vibration [5, 7, 8], wall deviation, and contour deviation, typically appear in the spinning process of thin-walled parts. The design of suitable spinning parameters is therefore particularly important to guarantee the forming quality of alloy parts [9, 10].

In recent years, a number of scholars have studied the metal sheet spinning of different parts by numerical simulations and experiments [1, 2, 11]. Metal sheet spinning can be divided into mandrel spinning and mandrel-free spinning depending on whether there is a specific mandrel in the spinning process [1, 2]. In the mandrel spinning process, Lin et al. [5, 7] obtained the optimal parameters of the staggered spinning for thin-walled Hastelloy C-276 cylindrical part, i.e., the three different roller fillet radii were determined as 3 mm, 4 mm and 6 mm, respectively,

✉ Yong-Cheng Lin
yclin@csu.edu.cn

¹ School of Mechanical and Electrical Engineering, Central South University, Changsha 410083, People's Republic of China

² State Key Laboratory of High Performance Complex Manufacturing, Changsha 410083, People's Republic of China

³ Light Alloy Research Institute, Central South University, Changsha 410083, People's Republic of China

and the roller feed ratio was approximately 0.8 mm/r. Xia et al. [6] found that the dynamic recrystallization behavior was enhanced with the increase in the forming temperature and total thinning ratio of wall thickness. Wang and Long [12] found that the wall thickness of the blank decreased in the forward pass and remained unchanged in the backward pass during multi-pass spinning. Zhan et al. [13] reported that the precision of wall thickness in cone spinning could be improved by increasing the feed ratio; however, it reduced the contour precision. El-Khabeery et al. [14] concluded that the dimensional precision of cylindrical aluminum cups was enhanced in conventional spinning as the roller angle and feed ratio were reduced. Xiao et al. [15] revealed that a large clearance between the roller and mandrel as well as a small feed ratio in asymmetric multi-pass spinning could improve wall thickness uniformity. Liu et al. [16] and Hayama et al. [17] discovered that the wall thickness distribution of final workpieces was determined by the first pass in conventional spinning. Xia et al. [18, 19] found that the spinning force was considerably affected by the feed ratio in hollow-part spinning, and it increased with the feed ratio. Kong et al. [20] observed that the feed ratio had a considerable influence on wrinkling, and a low feed ratio could reduce the possibility of its occurrence. Zhang et al. [21] indicated that the flange wrinkling of thin-walled vessel heads easily occurred when the ratio of sheet metal thickness to diameter was extremely small. Xia et al. [22] reported that a large feed ratio could easily induce metal sheet wrinkling in the one-path draw spinning process.

In the mandrel-free spinning, the dependence on the mandrel is eliminated, and the flexibility of conventional spinning is improved. Lin et al. [4] successfully manufactured the thin wall ellipsoidal Al alloy heads with the thickness and diameter of 4 mm and 2.29 m, respectively, by mandrel-free spinning. Zoghi et al. [23] discussed the effects of feed and roller contact start point on strain and residual stress distribution in dome forming of steel tube by spinning at an elevated temperature. Shima et al. [24] developed a die-less shear spinning method, which could be used for sheet metal forming. Rao et al. [25] proposed a multi-constraint spinning method for manufacturing large ellipsoidal parts without wrinkles and cracks and for achieving a wall thickness deviation of less than 10%. Kawai et al. [26, 27] developed a general-purpose mandrel spinning method to successfully manufacture hemispherical and conical shells. Kang et al. [28] discovered that shear spinning was the main deformation mode during the conventional spinning of plates, and wall thickness values conformed with the sine law. Han et al. [29] proposed a method to control the wall thickness distribution in the synchronous die-less shear spinning of oblique cones. Li et al. [30] claimed that a low-degree bending of concave roller paths could reduce contour deviation, and a high-

dimensional precision could be obtained with a low-degree bending of convex roller paths. Sekiguchi and Arai [31] discovered that various inclination angles of the flange could cause different wall thickness distributions during oblique shear spinning. Based on a quadratic Bezier curve, Polyblank and Allwood [32] proposed a parametric tool path planning method for metal sheet spinning. Jia et al. [33] found that the edge of the blank flange could easily wrinkle at the 0° area. Liu [34] found that the wrinkling deformation could remarkably increase the strain energy. Sugita and Arai [35] presumed that wrinkling easily occurred if rotational pass sets were employed to form rectangular box shapes.

The foregoing review reveals that mandrel spinning requires specific mandrels that limit its application [36]. Meanwhile, the dimensional precision of conventional mandrel-free spinning is not easy to control [37]. Moreover, thin-walled parts are prone to wrinkling during mandrel spinning or mandrel-free spinning and can be more severe in those with large diameter-to-thickness ratios [24]. In this work, a marginal-restraint mandrel-free spinning process that can effectively avoid wrinkling is proposed for the manufacture of thin-walled ellipsoidal heads. In addition, a finite element model (FEM) is established and verified to study the influences of spinning parameters on the wall thickness precision and contour precision of thin-walled ellipsoidal heads. Finally, the optimized spinning parameters are obtained and verified by experiments.

2 Marginal-restraint mandrel-free spinning process

Figure 1 shows the schematic of marginal-restraint mandrel-free spinning process. The process includes two passes. At the beginning of spinning, a blank is restrained on the cylindrical support fixture by the blank-hold ring that can preclude the deformation and wrinkling of metal sheet flange. Moreover, wrinkling, which can be reflected by the stress distribution in spun heads, is avoided in the forming regions. This aspect will be discussed in Section 3.2.2.

In the first pass (see Fig. 1a), the blank is rotated around the center axis of the fixture as the roller moves along the target contour. The blank is spun into a conical part with a large deformation as the roller moves along the 0–1–2–3–0 trajectory. The wall thickness can be evaluated as $t_1 = t_0 \cos \alpha$. Here, diameter D_0 is the upper limit of the forming range of the blank, and the spinning parameters, F , β , α , N , ρ_R , are the feed ratio, roller installation angle, forming angle, spindle speed, and roller fillet radius, respectively.

In the second pass (see Fig. 1b), the conical part is gradually expanded into a curved part with a relatively

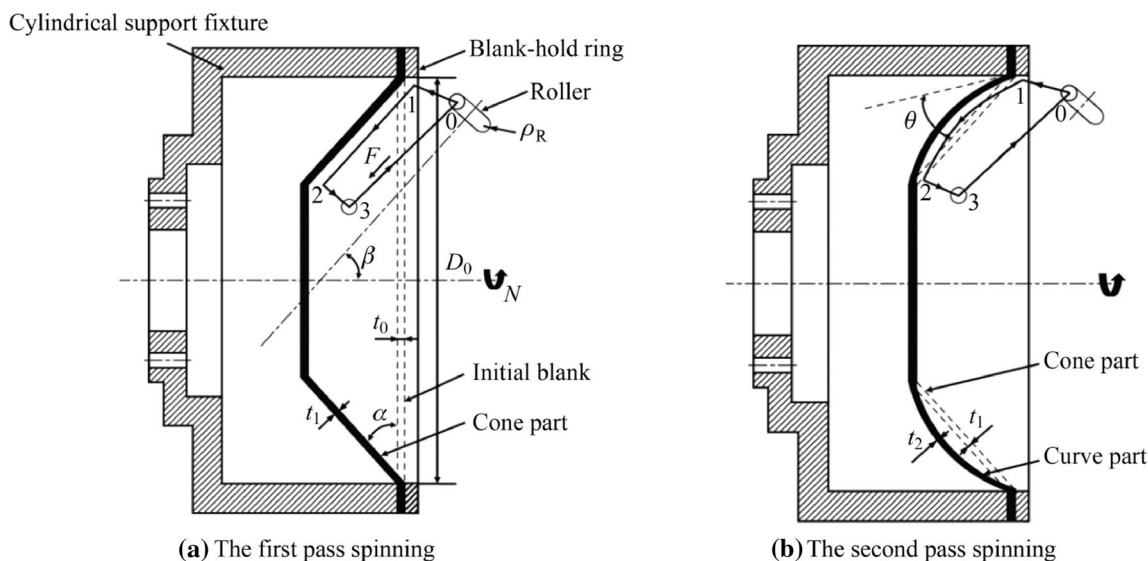


Fig. 1 Schematic diagrams of the marginal-restraint mandrel-free spinning process

small deformation and wall thickness variation. The wall thickness, t_2 , can be calculated by the principle of volume invariance. Furthermore, the roller motion direction of the second pass can be divided into forward motion (the roller moves along trajectory 0–1–2–3–0) and backward motion (along trajectory 0–3–2–1–0). The target contour of the curved part is reflected by the angle between passes (i.e., θ , the included angle between the contour tangent of the curved part and conical part profile). Additionally, the other spinning parameters (F , β , N , and ρ_R) of the second pass are the same as those of the first pass.

3 Development and verification of FEM

3.1 Development of FEM

The metal spinning process is a dynamic forming process with complex deformation mechanisms and contact conditions. In view of this, a three-dimensional (3D) dynamic explicit FEM is established based on the ABAQUS/Explicit code to simulate the marginal-restraint mandrel-free spinning process, as shown in Fig. 2a; X_1 and Y_1 are the two directions of roller movement. Figures 2b and c show the deformation process of each spinning pass in the simulation. Here, X and Y represent the radial and axial directions, respectively.

In this model, the cylindrical support fixture is simplified into a support ring, which is combined with the edge of the lower surface of the blank by the tie function in ABAQUS software. Meanwhile, the rotating boundary condition is set for the fixture to drive the rotation of the blank. The blank-holder ring is combined with the edge of

the upper surface of the blank to restrain the deformation of this edge. The motion of the roller in the X_1 and Y_1 directions are set to satisfy the feeding requirements of different target profiles in the spinning process, as shown in Fig. 2a. Furthermore, the roller, blank-holder ring, and support ring are all set as discrete rigid bodies to improve computing efficiency. The mass scaling factor of the model is set to 20.

The blank is defined as deformable and meshed with a continuous shell element (SC8R). The number of elements and nodes in the FEM are set as 10 448 and 19 284, respectively. The material of the blank, which is assumed to be homogeneous and isotropic, is a commercial 5052 aluminum alloy, and its properties are obtained by uniaxial tensile test, as listed in Table 1. The elastic capacity of the material is described by Hooke's law, and its plastic capacity is described by von Mises criterion and Hollomon's strain-hardening law, $\sigma = K\varepsilon^n$. The kinematic contact method of finite sliding formulation and Coulomb friction are used to simulate the contact behavior between the roller and blank. The Coulomb friction coefficient is set as 0.02 [12]. A springback analysis model is also established using ABAQUS/Standard after the spinning with ABAQUS/Explicit is simulated.

Wall thickness and contour characteristics are the two important geometric dimensions of thin-walled ellipsoidal heads. In order to study the influences of spinning parameters on wall thickness distribution and contour characteristics, orthogonal experimental schemes, $L_{16}(4^5)$ and $L_{18}(2 \times 3^5)$, are designed for the first and second passes, as summarized in Tables 2 and 3, respectively. Each spinning parameter is set as having four levels (1–2–3–4) in the first

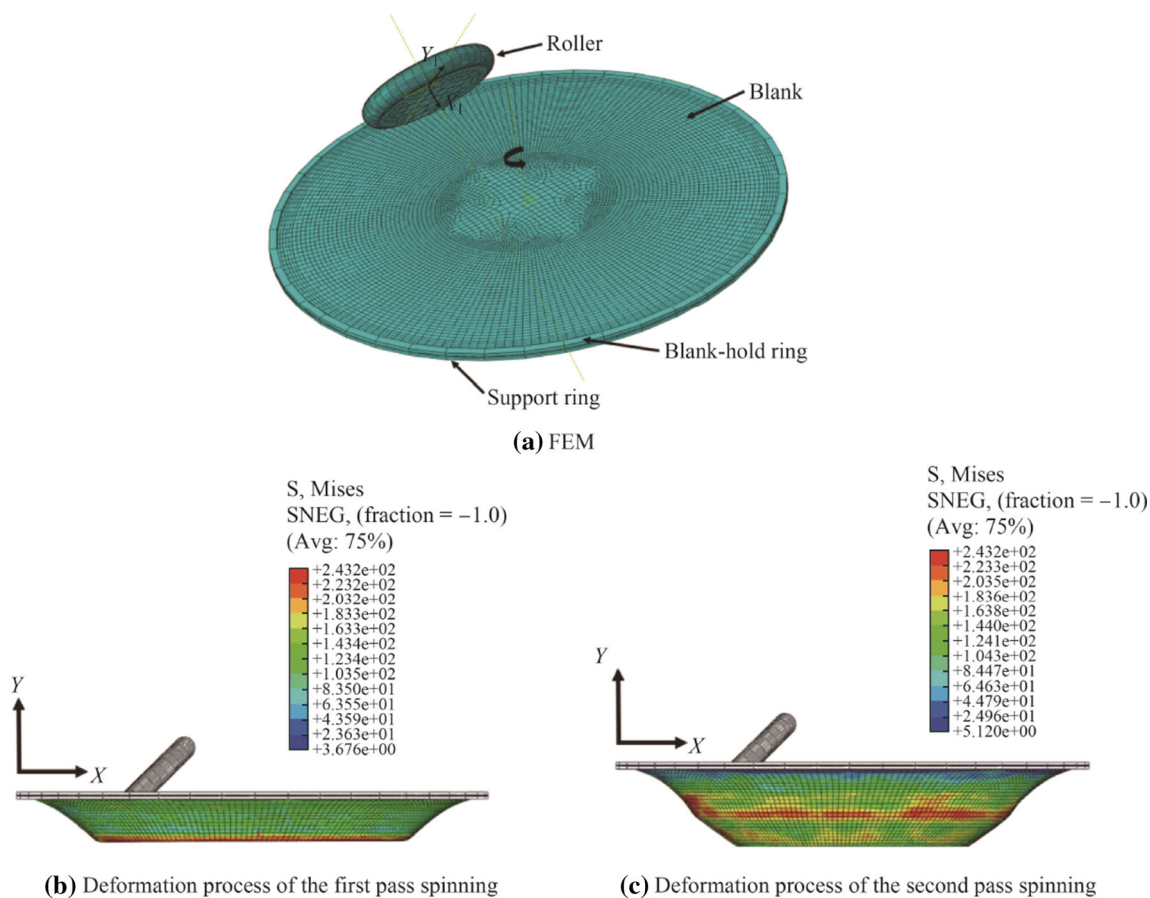


Fig. 2 Schematic diagrams of the FEM and deformation process of the spinning simulation

Table 1 Mechanical properties of 5052 aluminum alloy

Young's modulus/GPa	Poisson's ratio ν	Yield strength/MPa	Strength coefficient, K /MPa	Hardening exponent, n
61	0.33	163	343.53	0.151

pass and three levels (1–2–3) in the second pass. The level values successively increase.

3.2 Verification of FEM

3.2.1 Energy balance verification

Figure 3 shows the variations in energy ratios (kinetic energy/internal energy and artificial energy/internal energy) in the numerical simulations of two-pass spinning. It is found that in most spinning processes, the ratio of kinetic energy to internal energy is less than 10%, as shown in Fig. 3a. The ratio is initially high because the roller and blank have not been in contact, and there is practically no plastic deformation. Moreover, Fig. 3b shows that the ratio of artificial strain energy to internal energy is less than 5%.

This indicates that the influence of inertia resulting from mass scaling (see Section 3.1) is not significant on the simulation results, and the simulation precision is unaffected by the hour glassing problem [38]. The set of parameters of the FEM are therefore reasonable.

3.2.2 Experimental verification

The verification of the FEM based on experimental results is presented in this section. Figure 4a shows the spinning experimental equipment and the spun thin-walled ellipsoidal head. The experimental material has a 330 mm formable diameter and 1mm initial wall thickness. The main spinning parameters (i.e., α , β , N , F , and ρ_R) in the first pass are 40°, 45°, 360 r/min, 1.4 mm/r, and 8 mm, respectively. In the second pass, the angle between passes

Table 2 Orthogonal experiment scheme of the first pass spinning

Case	Forming angle $\alpha/(\circ)$	Roller installation angle $\beta/(\circ)$	Roller fillet radius $\rho_R/(\text{mm})$	Spindle speed $N/(\text{r}\cdot\text{min}^{-1})$	Feed ratio $F/(\text{mm}\cdot\text{r}^{-1})$
1	15	20	12	200	1.8
2	15	35	9	100	2.4
3	15	50	6	400	0.6
4	15	65	3	300	1.2
5	25	20	3	100	0.6
6	25	35	6	200	1.2
7	25	50	9	300	1.8
8	25	65	12	400	2.4
9	35	20	6	300	2.4
10	35	35	3	400	1.8
11	35	50	12	100	1.2
12	35	65	9	200	0.6
13	45	20	9	400	1.2
14	45	35	12	300	0.6
15	45	50	3	200	2.4
16	45	65	6	100	1.8

Table 3 Orthogonal experiment scheme of the second pass spinning

Case	Roller motion direction	Angle between passes $\theta/(\circ)$	Roller installation angle $\beta/(\circ)$	Roller fillet radius ρ_R/mm	Spindle speed $N/(\text{r}\cdot\text{min}^{-1})$	Feed ratio $F/(\text{mm}\cdot\text{r}^{-1})$
1	Backward	6	20	3	120	0.8
2	Backward	6	40	6	240	1.6
3	Backward	6	60	9	360	2.4
4	Backward	10	20	3	240	1.6
5	Backward	10	40	6	360	2.4
6	Backward	10	60	9	120	0.8
7	Backward	14	20	6	120	2.4
8	Backward	14	40	9	240	0.8
9	Backward	14	60	3	360	1.6
10	Forward	6	20	9	360	1.6
11	Forward	6	40	3	120	2.4
12	Forward	6	60	6	240	0.8
13	Forward	10	20	6	360	0.8
14	Forward	10	40	9	120	1.6
15	Forward	10	60	3	240	2.4
16	Forward	14	20	9	240	2.4
17	Forward	14	40	3	360	0.8
18	Forward	14	60	6	120	1.6

(θ) is 8° , and the other spinning parameters (β , N , F , and ρ_R) are the same as those in the first pass. Additionally, the motion of the roller in the second pass is directed backwards. The spun thin-walled ellipsoidal heads are shown in

Figs. 4b and c. It is evident that wrinkling has been avoided as indicated by the stress distributions in the simulated heads, as shown in Figs. 4d and e. After the first and second spinning passes, four stable stress regions are

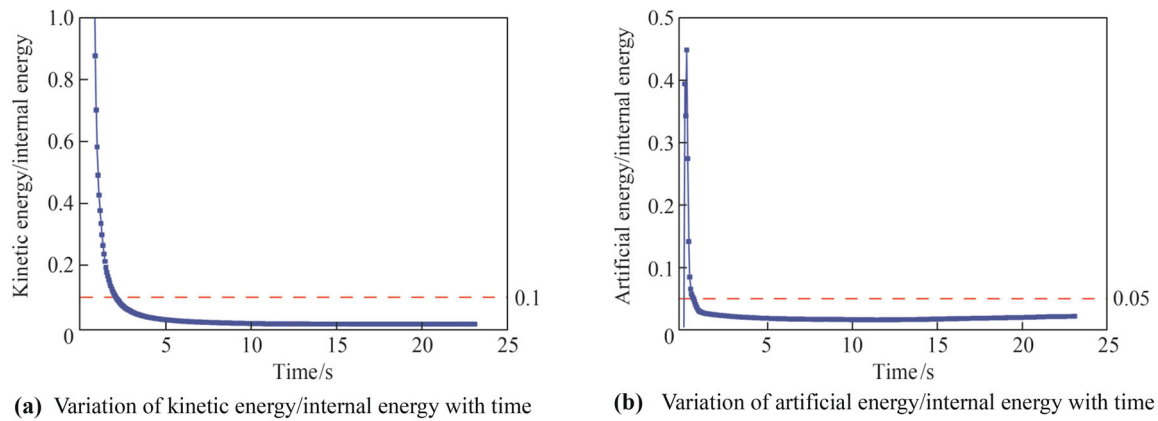


Fig. 3 Changes of energy ratios in numerical simulations

distributed on the forming workpiece surface. Here, the uniformly-distributed von Mises stress in the forming area is not large. Moreover, the red regions shown in Figs. 4d and e are the final positions of roller movements for the first and second passes, respectively. The von Mises stresses in these red regions are not extremely large, and the materials are uniformly distributed.

To analyze the dimensional precision, only half of the cross section is considered because the workpieces are axisymmetric. The thickness and contour are obtained from a single generatrix. Here, a 3D laser scanning measurement system named FARO is employed to obtain the contour data of the workpiece, whereas the wall thickness data are derived using a dual-ball micrometer. Figures 5a and b compare the simulated and experimental wall thicknesses of the first and second pass spun heads, respectively. It is found that the spinning stage can be divided into three spinning regions, i.e., initial, steady, and final spinning regions, which are similar to the wall thickness distributions of shear spun parts [39]. The steady spinning region where the change in wall thickness is not distinct is mainly discussed here. In the axial direction, the simulated wall thickness distribution is consistent with experimental results. The maximum errors between simulated and experimental results are 4.6% and 5.5% for the first and second passes, respectively. Figures 5c and d compare the simulated and experimental contours of the first and second pass spun heads, respectively. In the radial direction, the maximum errors between simulated and experimental results are 1.83% and 3.06% for the first and second passes, respectively; in the axial direction, these maximum errors for the first and second passes are 2.8% and 3.9%, respectively. These results indicate that the FEM can be effectively utilized to simulate the marginal-restraint mandrel-free spinning.

3.3 Dimensional precision of thin-walled spun heads

In this work, the wall thickness precision is characterized by the average deviation ratio of wall thickness (ADROWT, T) and the standard deviation of wall thickness (SDOWT, t'), as evaluated by Eqs. (1) and (2). Furthermore, the contour precision of the spun part is reflected by the deviation ratio of the forming angle (DROFA, $\Delta\alpha$) and average radial deviation (ARD, L'), as evaluated by Eqs. (3) and (4), respectively. Here, t_0 is the designed wall thickness; t is the simulated wall thickness; \bar{t} is the average wall thickness; n and n_2 are the numbers of extracted wall thickness and contour coordinates, respectively; α_0 is the designed forming angle; α is the forming angle of contour coordinate fitting; L and l are the simulated and designed contour coordinates, respectively. In addition, the degree of influence of spinning parameters on the above four indicators is characterized by the range obtained from orthogonal analysis.

$$T = \frac{1}{t_0} \left(\frac{1}{n} \sum_{i=1}^n t_i - t_0 \right) \times 100\%, \quad (1)$$

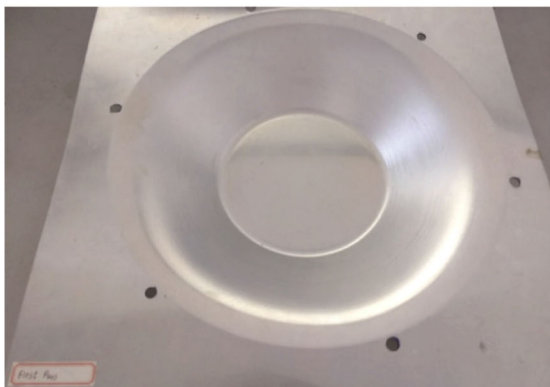
$$t' = \sqrt{\frac{1}{n} \sum_{i=1}^n (t_i - \bar{t})^2}, \quad (2)$$

$$\Delta\alpha = \frac{\alpha - \alpha_0}{\alpha_0} \times 100\%, \quad (3)$$

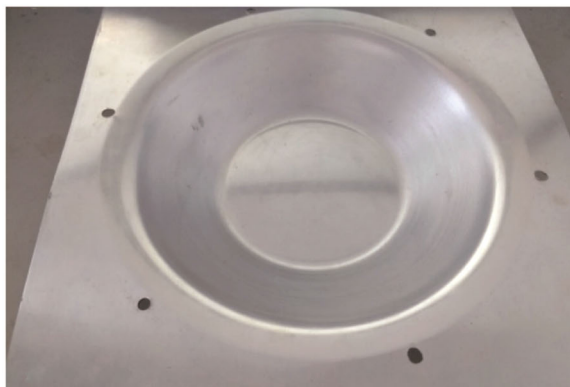
$$L' = \frac{1}{n_2} \sum_{i=1}^{n_2} |L_i - l_i|. \quad (4)$$



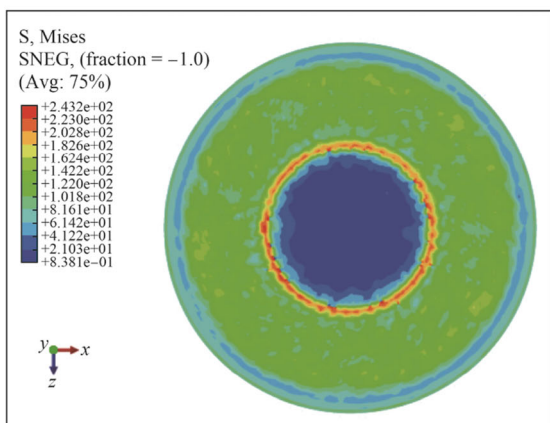
(a) Experimental setup



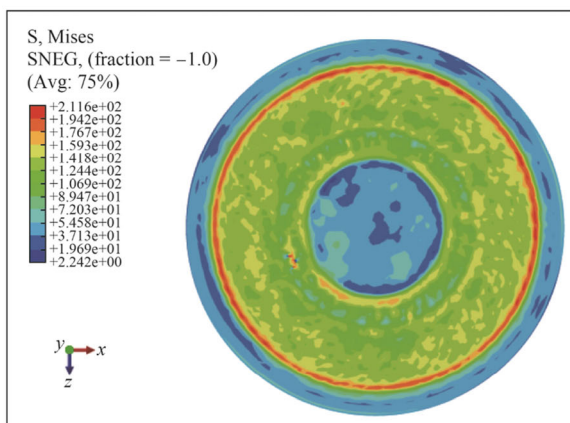
(b) The first pass spun head



(c) The second pass spun head



(d) Stress distribution of the first pass spun head



(e) Stress distribution of the second pass spun head

Fig. 4 Spinning experiments and the stress distributions of simulated heads

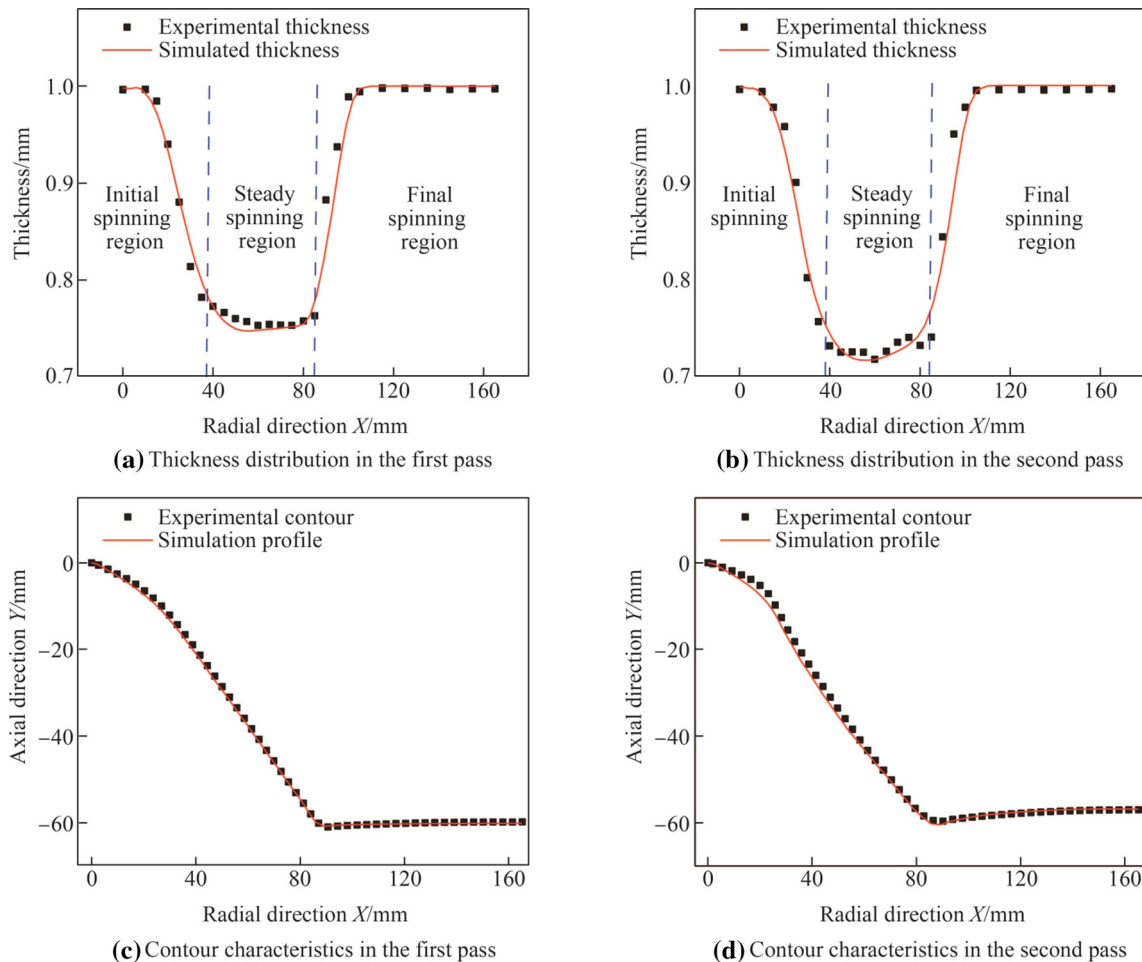


Fig. 5 Comparisons between the experimental and simulated results

4 Simulated results and discussion

4.1 Influences of spinning parameters on dimensional precision in the first pass

4.1.1 Influences of spinning parameters on wall thickness

Figure 6 illustrates the influences of spinning parameters on the ADROWT and SDOWT in the first pass spinning process. As shown in Figs. 6a and b, the influences of spinning parameters α , ρ_R and F on the ADROWT and SDOWT are relatively evident. For the ADROWT range, the values of α , ρ_R and F are evaluated as 6.5, 2.6, and 2.1 respectively, and for the SDOWT range, the parameter values are 0.005, 0.002, and 0.001, respectively. The small values of the roller installation angle, β , and spindle speed, N , however, indicate that the ADROWT and SDOWT values are not sensitive to these two parameters. The influences of spinning parameters α , ρ_R , and F , are therefore mainly discussed here. In Figs. 6c and d, it is clearly observed that both the ADROWT and SDOWT values

gradually rise when the forming angle or roller fillet radius is increased. This is because the larger forming angle easily induces a large wall thickness reduction ratio, which deteriorates the material flow stability and degrades the thinning precision of wall thickness. Additionally, the contact area between the roller and workpiece increases with increasing fillet radius, which hinders material flow in the axial direction. The suitable forming angle and roller fillet radius are found to be 15° and 3 mm, respectively. Moreover, as the feed ratio is continuously raised, the ADROWT and SDOWT values first decrease and then increase. At a given spindle speed, the contact time between the roller and workpiece generally increases with decreasing feed ratio. This increases the deformation degree, which then leads to an increasingly distinct wall thickness thinning; however, the deformation time is brief. If the feed ratio is extremely large (for example, 2.4 mm/r), then the plastic deformation will be insufficient, and wall thickness thinning will diminish. It is found that the suitable feed ratio is approximately 1.8 mm/r.

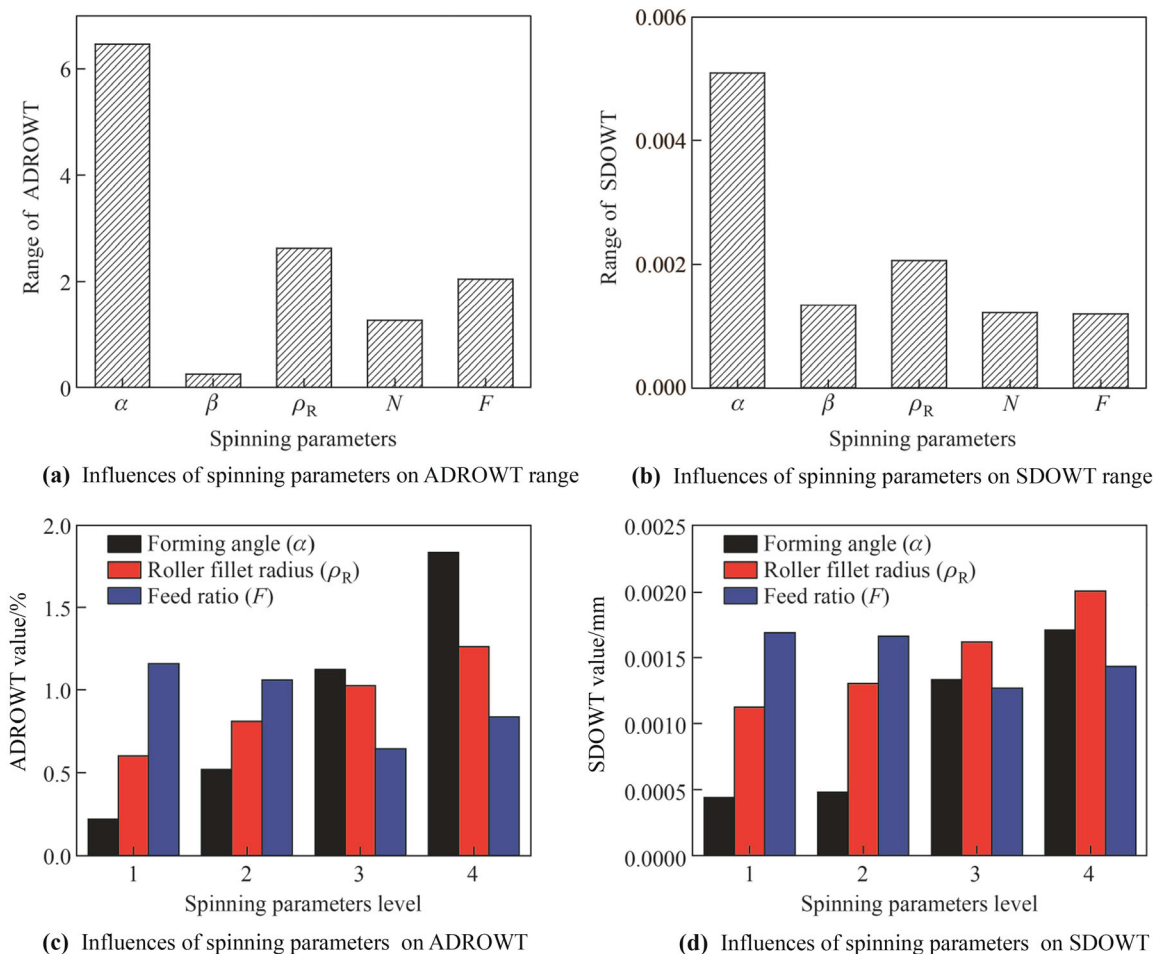


Fig. 6 Influences of spinning parameters on wall thickness in the first pass spinning process

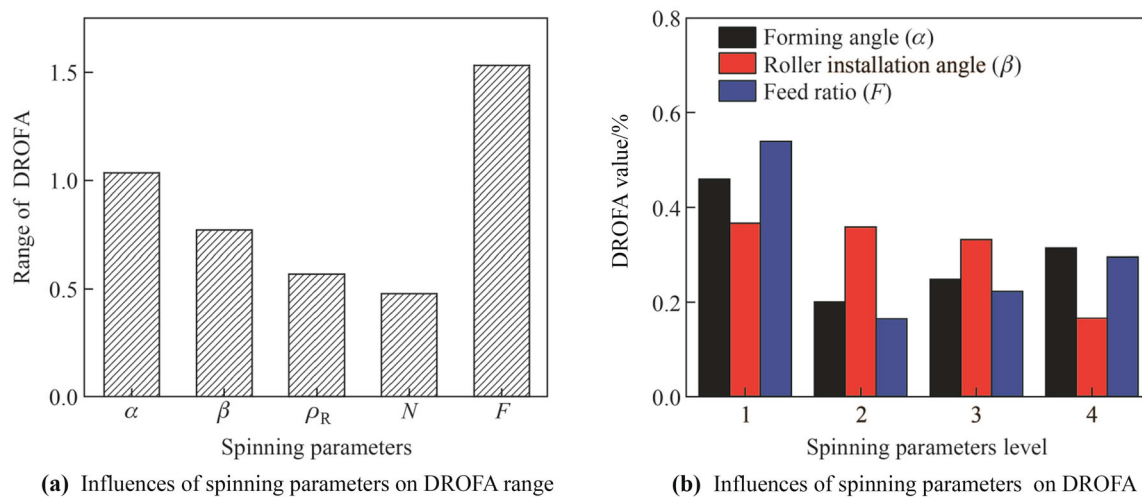


Fig. 7 Influences of spinning parameters on the contour precision in the first pass spinning process

4.1.2 Influences of spinning parameters on contour precision

Figure 7 displays the influences of spinning parameters on the contour precision in the first pass spinning process. As shown in Fig. 7a, the influences of spinning parameters α , β , and F on the DROFA are relatively evident. For the DROFA range, the values of α , β and F are evaluated as 1.04, 0.77 and 1.53 respectively. The relatively small values of roller fillet radius, ρ_R , and spindle speed, N , however, indicate that the DROFA value is not sensitive to these two parameters; accordingly, the influences of spinning parameters α , β , and F , are mainly discussed in this section. Figure 7b shows that the DROFA value first decreases and thereafter increases with the rise in the forming angle or feed ratio. This is because both shear and bending deformations occur in mandrel-free spinning [14]. A small forming angle increases the bending radius of workpieces that easily induces a large springback. The reduction in wall thickness is evident at a larger forming angle, which reduces material flowability and forming precision. A low feed ratio benefits the diameter expansion of workpieces, whereas a large feed ratio induces a large springback. The suitable forming angle and feed ratio are found to be 25° and 1.2 mm/r, respectively. In addition, the DROFA value first slowly decreases and then rapidly drops with increasing roller installation angle. This is because a large roller installation angle improves the material flow in the axial direction, making the shear deformation sufficient and reducing the springback. The suitable roller installation angle is accordingly found to be approximately 65° .

4.2 Influences of spinning parameters on dimensional precision in the second pass

4.2.1 Influences of roller motion direction on dimensional precision

Figure 8 displays the influences of roller motion direction on wall thickness and contour precision in the second pass spinning process. In Figs. 8a and b, it is clearly observed that the ADROWT value decreases, whereas the SDOWT value increases as the roller's motion direction is changed from backward to forward. This is because forward spinning promotes axial material flow and causes the contact region between the roller and workpiece to gradually decrease. This interpretation may be reflected by the changes in the spinning force, as shown in Fig. 8d. The contact area reduction in the forward spinning process decreases the spinning force, whereas the spinning force of backward spinning is relatively stable because of the small change in the contact area [18, 19]. Thereafter, the workpieces cannot be sufficiently deformed in the middle and later stages of forward spinning,

causing poor wall thickness uniformity and thinning degree. In view of the small difference in the theoretical wall thickness between the first and second passes, however, the low thinning degree of wall thickness reduces the ADROWT value. In addition, because of the insufficient workpiece deformation, the ARD value in the forward spinning process is also larger than that in the backward spinning process, as shown in Fig. 8c. As a result, the contour precision in the forward spinning process deteriorates. Accordingly, the suitable roller motion direction is backwards.

4.2.2 Influences of major spinning parameters on wall thickness

Figure 9 illustrates the influences of spinning parameters on wall thickness in the second pass spinning process. As shown in Figs. 9a and b, the influences of spinning parameters θ , β and F on the ADROWT and SDOWT values are also relatively considerable. For the ADROWT range, the values of θ , β and F are evaluated as 0.81, 0.27, and 0.33, respectively, and for the SDOWT range, these are 0.0055, 0.001 and 0.0014, respectively. The influences of the roller fillet radius, ρ_R , and spindle speed, N , on the ADROWT and SDOWT values are not considerable. In this section, therefore, the influences of θ , β and F , are mainly discussed. Figures 9c and d show that the ADROWT and SDOWT values sharply rise with the increase in the angle between passes or the decrease in the feed ratio. This trend is related to the degree of material deformation, as presented in Section 4.1.1. The suitable angle between passes and feed ratio are found to be 6° and 2.4 mm/r, respectively. In addition, the ADROWT and SDOWT values first increase and then slightly decrease as the roller installation angle is continuously increased. This is because a small roller installation angle can increase the workpiece radial strain, which is conducive for reducing wall thickness. A large roller installation angle induces a larger spinning force axial component, which enhances the wall thickness thinning effect. The appropriate roller installation angle is accordingly found to be approximately 20° .

4.2.3 Influences of major spinning parameters on contour precision

Figure 10 displays the influences of spinning process parameters on the contour precision in the second pass. As shown in Fig. 10a, the influences of spinning parameters θ , β and ρ_R on the ARD value are relatively considerable; for the ARD range, the parameter values are 0.42, 0.2 and 0.15, respectively. It can be found, however, that the ARD value is not sensitive to the spindle speed, N , and feed ratio, F , whose values are relatively small. Accordingly, the influences of θ , β and ρ_R are mainly discussed in this section. In Fig. 10b, it is clearly observed that the ARD

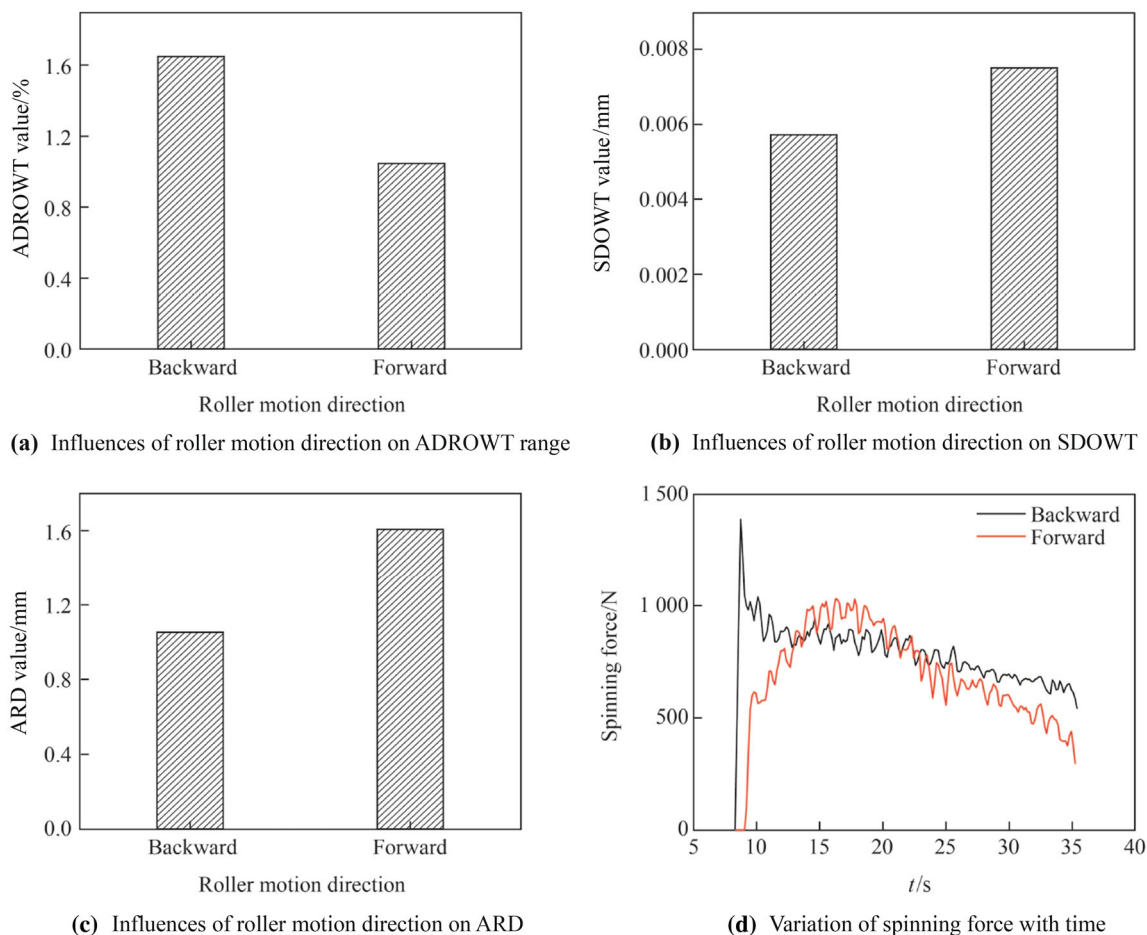


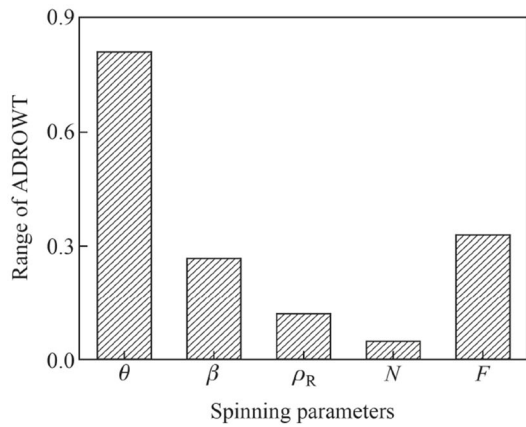
Fig. 8 Influences of roller motion direction on dimensional precision in the second pass pinning process

value first slightly decreases and then increases with the rise in the roller installation angle or roller fillet radius. This is because the small roller installation angle can increase the workpiece radial strain, which can improve the diameter expansion of the workpiece. A large roller installation angle enhances the axial material flow and easily causes a larger depth deviation; thereafter, the contour precision deteriorates. Moreover, a small roller fillet radius can reduce the contact area between the roller and workpiece, thus increasing the material axial flow and aggravating the depth deviation of the workpiece. The material axial flow is reduced when a larger roller fillet radius is used, resulting in the insufficient deformation of the material. The suitable roller installation angle and roller fillet radius are accordingly found to be 40° and 6 mm, respectively. The ARD value also gradually increases with the increase in the angle between passes. This is because a large angle between passes increases the wall thickness thinning degree, which deteriorates material flowability and forming precision. The suitable angle between passes is found to be approximately 6° .

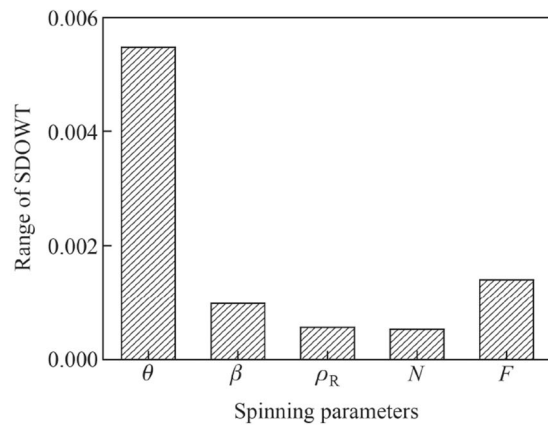
4.3 Verification of optimized spinning parameters

In the orthogonal experimental scheme, which involves the comprehensive consideration of wall thickness precision and contour precision, the optimized values of spinning parameters α , β , F and ρ_R for the first pass spinning process are approximately 25° , 65° , 1.8 mm/r, and 3 mm, respectively. For the second pass, the optimized values of α , β , F and ρ_R are approximately 6° , 20° , 2.4 mm/r, and 6 mm, respectively. Moreover, the selected roller motion direction for the second pass spinning process is backwards. The spinning experiments on thin-walled ellipsoidal heads are performed to validate the reliability of optimized spinning parameters. Here, the spindle speed, N , is maintained at 300 r/min.

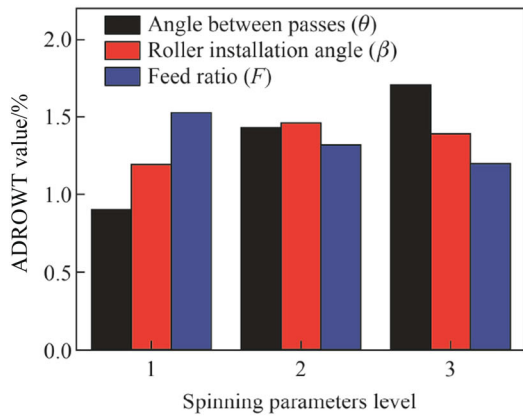
Figure 11 shows the spun thin-walled ellipsoidal heads formed by using unsuitable spinning parameters, such as a large forming angle (more than 55°) or feed ratio (more than 2.8 mm/r); some cracks and large ripples are evident. On the contrary, it can be observed that wrinkling is effectively avoided, and if the optimized spinning parameters are used, the surface quality of spun heads is ideal, as shown in



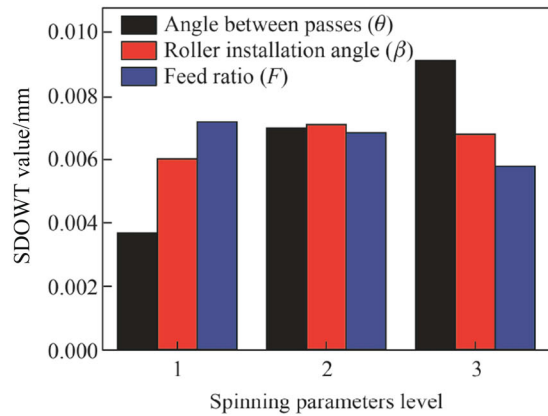
(a) Influences of spinning parameters on ADROWT range



(b) Influences of spinning parameters on SDOWT range

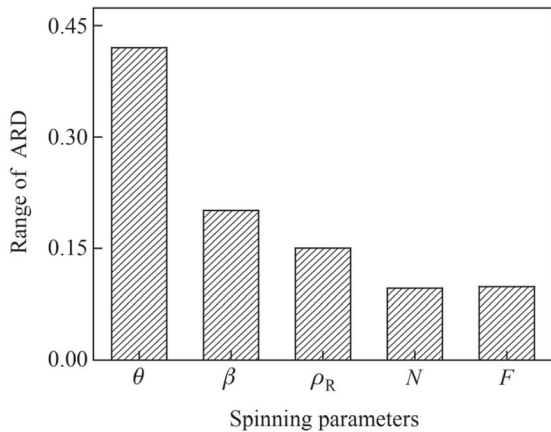


(c) Influences of spinning parameters on ADROWT

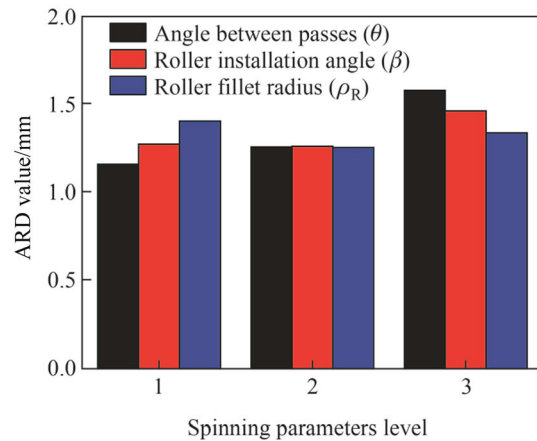


(d) Influences of spinning parameters on SDOWT

Fig. 9 Influences of spinning parameters on wall thickness in the second pass spinning process



(a) Range of ADR

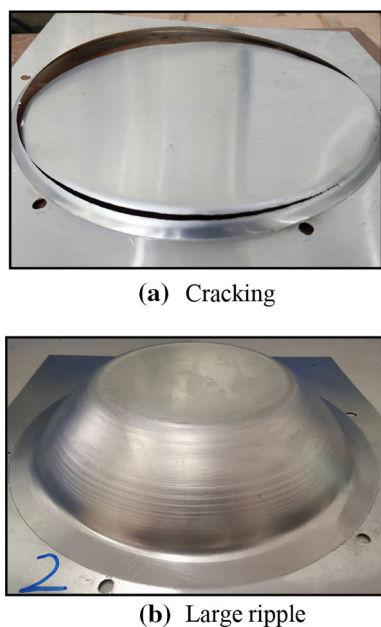


(b) Influences of spinning parameters on ADR

Fig. 10 Influences of spinning parameters on contour precision in the second pass spinning process

Figs. 12a and b. Figure 12c compares the experimental and designed wall thickness distributions. It can be seen that the experimental wall thickness in each pass approximates the designed thickness. It is evident that the ADROWT values in both passes are less than 0.5%. The SDOWT values in the

first and second spinning passes are 0.0014 mm and 0.0017 mm, respectively. In Fig. 12d, it is clearly observed that the experimental contour characteristics considerably coincide with the designed values. The DROFA value in the first pass spinning is less than 0.5%, and the ARD value in the second



(a) Cracking

(b) Large ripple

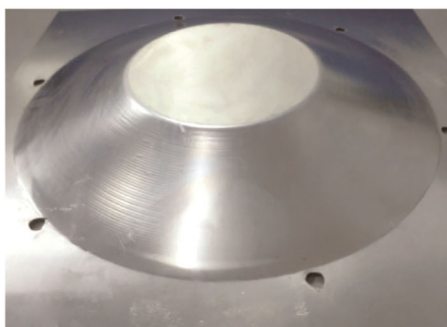
Fig. 11 Spun thin-walled ellipsoidal heads based on the unsuitable spinning parameters

pass spinning is 0.805 3 mm. The optimized spinning parameters can therefore be effectively employed to fabricate thin-walled ellipsoidal heads.

5 Conclusions

In this work, a marginal-restraint mandrel-free spinning process for the fabrication of thin-walled ellipsoidal heads without wrinkles is proposed. Moreover, an FEM is established to study the influences of spinning parameters on the wall thickness and contour characteristics of spun parts. Some crucial conclusions are summarized as follows.

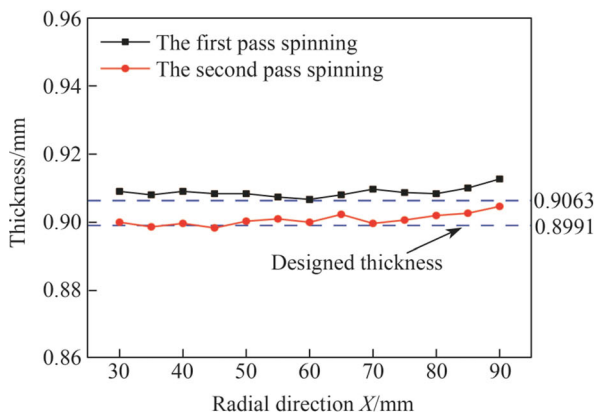
- (i) In the first pass spinning process, the wall thickness precision decreases with the increase in the forming angle or roller fillet radius, whereas it first increases and then decreases with the increase in feed ratio. The contour precision first increases and then decreases with the increase in the forming angle or feed ratio. The high roller installation angle can enhance the contour precision.
- (ii) In the second pass spinning process, the wall thickness precision decreases with the increase in the angle between passes or the decrease in feed ratio, whereas it first decreases and then increases with the increase in the roller installation angle. The contour precision first increases and then decreases with the increase in the roller installation angle or



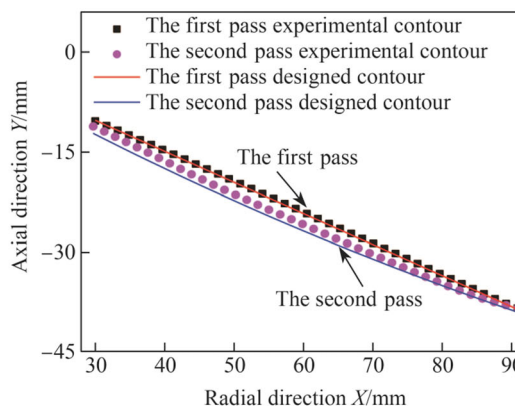
(a) The first pass spun head



(b) The second pass spun head



(c) Wall thickness distribution



(d) Contour characteristics

Fig. 12 Experimental results based on the optimized spinning parameters

roller fillet radius. The increase in the angle between passes can decrease the contour precision.

- (iii) For the first pass spinning, the optimized forming angle, roller installation angle, feed ratio, and roller fillet radius are approximately 25° , 65° , 1.8 mm/r, and 3 mm, respectively. For the second pass spinning, the suitable roller motion direction is backwards, and the optimized angle between passes, roller installation angle, roller fillet radius, and feed ratio are approximately 6° , 20° , 6 mm, and 2.4 mm/r, respectively.

Acknowledgements This work was supported by the National Natural Science Foundation of China (Grant No. 51775564), the 973 program (Grant No. 2014CB046600), and the Fundamental Research Funds for the Central Universities of Central South University (Grant No. 2019zzts946).

References

- Xia QX, Xiao GF, Long H et al (2014) A review of process advancement of novel metal spinning. *Int J Mach Tools Manuf* 85:100–121
- Wong CC, Dean TA, Lin J (2003) A review of spinning, shear forming and flow forming processes. *Int J Mach Tool Manuf* 43(14):1419–1435
- Zhang Q, Zhang C, Zhang MJ et al (2015) Research of net-shape power spinning technology for poly-V grooved aluminum pulley. *Int J Adv Manuf Technol* 81(9/12):1601–1618
- Lin YC, Wu Q, He DG et al (2020) Effects of solution time and cooling rate on microstructures and mechanical properties of 2219 Al alloy for a larger spun thin-wall ellipsoidal head. *J Mater Res Technol*. <https://doi.org/10.1016/j.jmrt.2020.01.095>
- Lin YC, Qian SS, Chen XM et al (2019) Staggered spinning of thin-walled Hastelloy C-276 cylindrical parts: numerical simulation and experimental investigation. *Thin Wall Struct* 140:466–476
- Xia Q, Long JC, Zhu NY et al (2019) Research on the microstructure evolution of Ni-based superalloy cylindrical parts during hot power spinning. *Adv Manuf* 7(1):52–63
- Lin YC, Qian SS, Chen XM et al (2020) Influences of feed rate and wall thickness reduction on the microstructures of thin-walled Hastelloy C-276 cylindrical parts during staggered spinning. *Int J Adv Manuf Technol* 106(9/10):3809–3821
- Zhang HR, Zhan M, Guo J et al (2019) Forming the transverse inner rib of a curved generatrix part through power spinning. *Adv Manuf* 7(1):105–115
- Huang CQ, Liu JX (2020) Effects of hot spinning and heat treatment on the microstructure, texture, and mechanical properties of A356 wheel hubs. *Metall Mater Trans A* 51:289–298
- Saied EK, El-Abden SZ, Abd-Eltwab AA et al (2019) Combining conventional spinning with wall thickness reduction in one pass. *Int J Mech Prod Eng Res Dev* 9(3):1429–1436
- Liu CH (2007) Dynamic finite element modeling for the conventional spinning process. *J Chin Inst Eng* 30(5):911–916
- Wang L, Long H (2011) Investigation of material deformation in multi-pass conventional metal spinning. *Mater Des* 32(5):2891–2899
- Zhan M, Yang H, Zhang JH et al (2007) 3D FEM analysis of influence of roller feed ratio on forming force and quality of cone spinning. *J Mater Process Technol* 187/188:486–491
- El-Khabeery MM, Fattouh M, El-sheikh MN et al (1991) On the conventional simple spinning of cylindrical aluminium cups. *Int J Mach Tools Manuf* 31(2):203–219
- Xiao Y, Han Z, Fan ZJ et al (2018) A study of asymmetric multi-pass spinning for angled-flange cylinder. *J Mater Process Technol* 256:202–215
- Liu JH, Yang H, Li YQ (2002) A study of the stress and strain distribution of first-pass conventional spinning under different roller-traces. *J Mater Process Technol* 129(1):326–329
- Hayama M, Kudo H, Shinokura T (1970) Study of the pass schedule in conventional simple spinning. *Bull Jpn Soc Mech Eng* 13(65):1358–1365
- Xia QX, Wang YP, Yuan N et al (2011) Study on spinning of pentagonal cross-section hollow-part based on orthogonal experiment design. *Adv Mater Res* 314/316:783–788
- Xia QX, Lai ZY, Long H et al (2013) A study of the spinning force of hollow parts with triangular cross sections. *Int J Mach Tools Manuf* 68(9/12):2461–2470
- Kong Q, Yu Z, Zhao Y et al (2017) Theoretical prediction of flange wrinkling in first-pass conventional spinning of hemispherical part. *J Mater Process Technol* 246:56–68
- Zhang YQ, Shan DB, Xu WC et al (2010) Study on spinning process of a thin-walled aluminum alloy vessel head with small ratio of thickness to diameter. *J Manuf Sci Eng* 132(1):014504
- Xia QX, Shima S, Kotera H et al (2005) Study of the one-path deep drawing spinning of cups. *J Mater Process Technol* 159(3):397–400
- Zoghi H, Arezoodar AF, Sayeefabi M (2012) Effect of feed and roller contact start point on strain and residual stress distribution in dome forming of steel tube by spinning at an elevated temperature. *Proc IMechE Part B J Eng Manuf* 226:1880–1890
- Shima S, Kotera H, Murakami H et al (1997) Development of flexible spin-forming method. *J Jpn Soc Technol Plastic* 38:40–44
- Rao GJ, Li XH, Zhou L et al (2018) A multi-constraint spinning process of ellipsoidal heads. *Int J Adv Manuf Technol* 94(1/4):1505–1512
- Kawai K, Yang LN, Kudo H (2007) A flexible shear spinning of axi-symmetrical shells with a general-purpose mandrel. *J Mater Process Technol* 192:13–17
- Kawai K, Yang LN, Kudo H (2001) A flexible shear spinning of truncated conical shells with a general-purpose mandrel. *J Mater Process Technol* 113(1/3):28–33
- Kang DC, Gao XC, Meng XF et al (1999) Study on the deformation mode of conventional spinning of plates. *J Mater Process Technol* 91(1/3):226–230
- Han ZR, Fan ZJ, Xiao Y et al (2017) A research on thickness distribution of oblique cone in mandrel-free shear spinning. *Int J Adv Manuf Technol* 90:2901–2912
- Li Y, Wang J, Lu GD et al (2014) A numerical study of the effects of roller paths on dimensional precision in mandrel-free spinning of sheet metal. *J Zhejiang Univ-Sci A* 15(6):432–446
- Sekiguchi A, Arai H (2012) Control of wall thickness distribution by oblique shear spinning methods. *J Mater Process Technol* 212(4):786–793
- Polyblank JA, Allwood JM (2015) Parametric toolpath design in metal spinning. *CIRP Ann* 64(1):301–304
- Jia Z, Han ZR, Liu BM (2017) Numerical simulation and experimental study on the non-axisymmetric mandrel-free shear spinning. *Int J Adv Manuf Technol* 92(1/4):497–504
- Liu CH (2007) The simulation of the multi-pass and die-less spinning process. *J Mater Process Technol* 192/193:518–524
- Sugita Y, Arai H (2015) Formability in synchronous multipass spinning using simple pass set. *J Mater Process Technol* 217:336–344
- Imamura Y, Ikawa K, Sakane Y et al (2017) Investigation of forming accuracy in mandrel-free hot-spinning. *Procedia Eng* 207:1701–1706

37. Guo H, Wang J, Lu G et al (2017) A study of multi-pass scheduling methods for die-less spinning. *J ZheJiang Univ-Sci A* 18(6):413–429
38. User's Manual (2012) ABAQUS analysis user's manual. ABAQUS Inc version 6:12–3
39. Han D, Zhan M, Yang H (2013) Deformation mechanism of TA15 shells in hot shear spinning under various load conditions. *Rare Metal Mat Eng* 42(2):243–248



Y. C. Lin is a professor in the School of Mechanical and Electrical Engineering, Central South University, China. He received his B.S. (2000) and M.S. (2003) degrees from Liaoning University of Petroleum and Chemical Technology, China and his Ph.D. (2006) from Tianjin University, China; all his degrees are in Mechanical Engineering. He joined the faculty of Central South University in 2006. He is also a member of the State Key Laboratory of High Performance Complex Manufacturing.

His current research interests are experimental, theoretical, and simulation investigations on hot deformation processing–structure–property relationship of alloys. He has jointly published more than 180 international journal papers as well as two books. He has gained more than 10,000 self-exclusive citations. Moreover, he has obtained more than 30 patents in China and received four science and technology awards from Hunan Province, China. He is also a member of the editorial board of more than 10 international journals including *Materials and Design*, *Journal of Materials: Design and Applications*, *Materials Science and Engineering A*, *Materials*, *Journal of Materials Engineering and Performance*, and *Advanced Engineering Materials*. Additionally, he has been a chair and member of technical and organizing committees for more than 80 international academic conferences. Further details about him can be found at <http://faculty.csu.edu.cn/yclin>.



Jia-yang Chen is an M.S. candidate of the School of Mechanical and Electrical Engineering, Central South University, China. He obtained his B.S. degree in Materials Engineering from Xiangtan University, China. His main research interest is on advanced spinning processing technology of high-quality metal parts.



His current research interest is on hot deformation processing–structure–property relationship of alloys. He has jointly published more than 30 international journal papers.



Xin-He Li is a professor in the School of Mechanical and Electrical Engineering, Central South University, China. He is also a member of the State Key Laboratory of High Performance Complex Manufacturing. He received his B.S. degree (1984) in Mechanical Engineering from Central South University of Technology, China. He joined the faculty of Central South University in 2019. His current research interest is on advanced spinning processing technology of high quality metal parts. He has jointly published more than 50 scientific papers, and gained more than 20 patents in China.



Jian Yang obtained his M.S. degree in Mechanical Engineering from Central South University, China in 2018 and his B.S. degree in Mechanical Engineering from Qingdao University of Technology, China in 2015. His main research interest is on advanced spinning processing technology of high quality metal parts. He currently works with China Railway Construction Heavy Industry Co., Ltd.